Spatial stability of similarity solutions for viscous flows in channels with porous walls

Sergio Ferro, and Graciela Gnavi

Citation: Physics of Fluids **12**, 797 (2000); doi: 10.1063/1.870336
View online: https://doi.org/10.1063/1.870336
View Table of Contents: http://aip.scitation.org/toc/phf/12/4
Published by the American Institute of Physics

Spatial stability of similarity solutions for viscous flows in channels with porous walls

Sergio Ferro and Graciela Gnavi
Instituto de Física del Plasma, Consejo Nacional de Investigaciones Científicas y Técnicas, and Departamento de Física, Facultad de Ciencias Exactas y Naturales, Universidad de Buenos Aires, Ciudad Universitaria, Pabellón 1, 1428 Buenos Aires, Argentina

(Received 2 August 1999; accepted 19 November 1999)

The spatial stability of similarity solutions for an incompressible fluid flowing along a channel with porous walls and driven by constant uniform suction along the walls is analyzed. This work extends the results of Durlofsky and Brady [Phys. Fluids **27**, 1068 (1984)] to a wider class of similarity solutions, and examines the spatial stability of small amplitude perturbations of arbitrary shape, generated at the entrance of the channel. It is found that antisymmetric perturbations are the best candidates to destabilize the solutions. Temporally stable asymmetric solutions with flow reversal presented by Zaturska, Drazin, and Banks [Fluid Dyn. Res. **4**, 151 (1988)] are found to be spatially unstable. The perturbed similarity solutions are also compared with fully bidimensional ones obtained with a finite difference code. The results confirm the importance of similarity solutions and the validity of the stability analysis in a region whose distance to the center of the channel is more than three times the channel half-width. © *2000 American Institute of Physics.* [S1070-6631(00)02003-1]

I. INTRODUCTION

The Navier–Stokes equation for an incompressible viscous flow along a channel with porous walls, driven by constant uniform suction, admits a similarity solution. This solution was studied in 1953 by Berman,[1] who reduced the bidimensional Navier–Stokes equation to a fourth order nonlinear ordinary differential equation with two boundary conditions at each wall. This equation depends on a sole nondimensional parameter, the transversal Reynolds number, R, defined in terms of the channel width and the suction velocity. Similarity solutions were tested in early experiments on laminar flows in ducts with wall injection, where evidence of good agreement between measurements and theoretical predictions was reported.[2]

Many authors have studied Berman's equation (see, for example, Refs. 3–12) and found a very rich structure of solutions. Zaturska *et al.*,[8] however, proved that most of these solutions are temporally unstable to linear perturbations. On the other hand, the spatial stability of the solutions has not been completely analyzed. In 1984 Durlofsky and Brady[13] studied the spatial stability of *symmetric* solutions under linear *symmetric* perturbations.

This work presents the spatial stability analysis for both symmetric and asymmetric solutions under arbitrary small amplitude perturbations. The basic equations of the problem are shown in the next section and the stability analysis is developed in Sec. III. A comparison between the spatially perturbed similarity solutions and fully bidimensional ones is presented in Sec. IV. Section V is devoted to the conclusions.

II. BASIC EQUATIONS

The coordinate system of Fig. 1 is considered, with the origin in the center of the channel and the x-axis parallel to the walls. The parameters of the problem are the suction velocity V, the channel width $2h$, ρ and μ the (constant) density and viscosity of the fluid, respectively. Steady state solutions for the nondimensional velocity and pressure fields $\underline{u}(x,y)$, $p(x,y)$ satisfy the continuity and Navier–Stokes equations. Thus,

$$\begin{aligned} &\mathrm{div}(\underline{u})=0,\\ &\underline{u}-\mathrm{grad}(\underline{u})=-\mathrm{grad}(p)+\mathrm{div}(\mathrm{grad}(\underline{u}))/R, \end{aligned} \tag{1}$$

with $\underline{u}=\pm\hat{y}$ on the walls. The unit vectors in the x and y directions are denoted by $\hat{x}$ and $\hat{y}$, respectively. The transversal Reynolds number is $R=Vh\rho/\mu$. The variables are expressed in units of the length h, the velocity V and the pressure $V^2\rho$.

A similarity solution of the form,

$$\begin{aligned} &\underline{u}(x,y)=x\frac{\partial f(y)}{\partial y}\hat{x}-f(y)\hat{y},\\ &p(x,y)=\pi(y)+Ax^2/2, \end{aligned} \tag{2}$$

leads to the following equation for $f(y)$:

$$f^{iv}+R(ff'''-f'f'')=0, \tag{3}$$

where $'$ denotes differentiation along the transversal coordinate. The boundary conditions for $f(y)$ are

$$f(1)=-1,\ f(-1)=1,\ f'(1)=0,\ f'(-1)=0.$$

Once Eq. (3) is solved, the pressure field corresponding to Eq. (2) can be obtained from the following expressions:

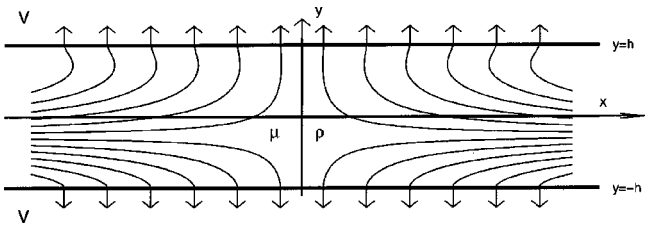

FIG. 1. Channel diagram and coordinate system. The plotted stream lines represent the flow pattern of an asymmetric similarity solution of the Navier–Stokes equation.

$$\pi(y)=\pi(1)+(1-f^2)/2-f'/R,$$

$$A=(ff''-f'^2)+f'''/R.$$

A spectral[14] code was developed to obtain numerical solutions for the flow equation (3). The results obtained were in good agreement with those presented by Zaturska, Drazin, and Banks in Ref. 8. In Fig. 2, a bifurcation diagram is presented showing the different steady state solutions of Eq. (3). In this diagram each solution is represented by the value $f''(1)$, which is proportional to the viscous stress at the wall $y=1$. Several branches of solutions and bifurcations appear in the diagram. The asymmetric solutions are plotted with dotted lines. There is a stable symmetric solution (denoted solution of type I) which loses its stability at $R_{\mathrm{I}}=6.001$, where two stable asymmetric solutions (types I_a and I'_a) are generated in a pitchfork bifurcation. These solutions remain stable below $R_{\mathrm{I}a}=12.963$, where a Hopf bifurcation takes place. A saddle-node bifurcation at $R_{\mathrm{II}}=12.165$ gives birth to two temporally unstable symmetric solutions (types II and III) one of which undergoes a pitchfork bifurcation at $R_{\mathrm{III}}=15.415$, generating two new asymmetric branches (types III_a and III'_a). As $R\to\infty$, solutions of type I and II differ by exponentially small terms only,[7] and they coalesce in a cusp type bifurcation.

Solutions of type II with $R<R'_{\mathrm{II}}=13.119$ and those of type III, III_a, and III'_a have regions of flow reversal in the center of the channel. Solutions of type I_a and I'_a have a region of flow reversal near one wall if $R>R'_{\mathrm{I}a}=6.557$.

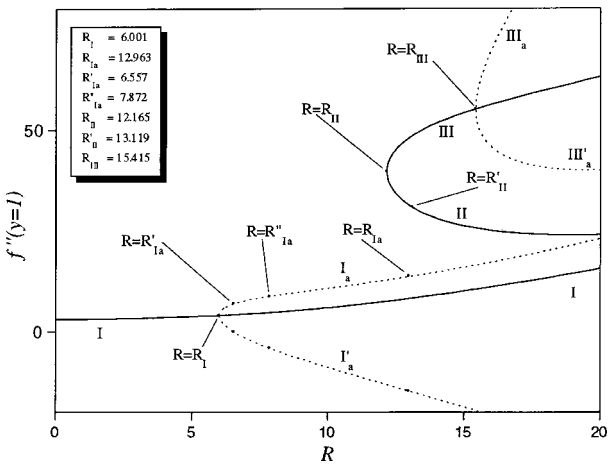

FIG. 2. Bifurcation diagram showing symmetric (full lines) and asymmetric (dotted lines) solutions of Eq. (3).

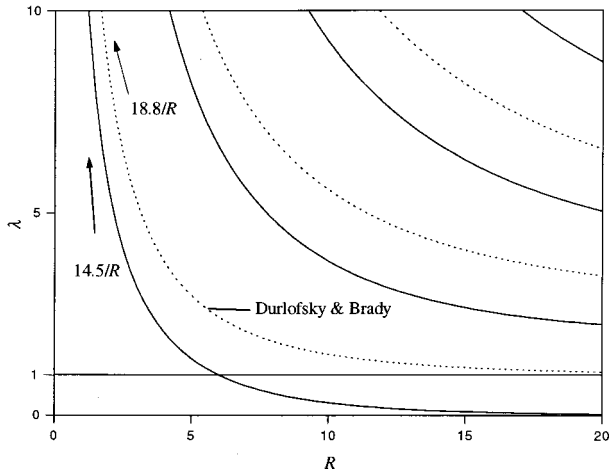

FIG. 3. Eigenvalues of symmetric (type I) solutions of Eq. (3). Full lines correspond to antisymmetric eigenfunctions and dotted lines to symmetric ones.

III. SPATIAL STABILITY ANALYSIS

The spatial stability analysis of Eq. (3) was performed taking solutions of the form $\tilde{f}(x,y)=xf(y)+x^{\lambda}H_{\lambda}(y)$ for the stream function. The term $x^{\lambda}H_{\lambda}(y)$ is regarded as a perturbation to the similarity solution. The linearized approximation for $H_{\lambda}(y)$, valid in the region not close to the center of the channel, leads to the following characteristic value problem:

$$H_{\lambda}^{iv}+R(fH_{\lambda}'''-f''H_{\lambda}')=\lambda R(f'H_{\lambda}''-f'''H_{\lambda}), \tag{4}$$

with homogeneous boundary conditions,

$$H_{\lambda}(-1)=H_{\lambda}'(-1)=H_{\lambda}(1)=H_{\lambda}'(1)=0. \tag{5}$$

For a given Reynolds number, the existence of characteristic values λ with $\mathrm{Re}(\lambda)<1$, implies the instability of the similarity solution. Under these conditions certain perturbations at the mouth of the channel can grow downstream, destroying the similarity solution in the interior.

This kind of analysis (for symmetric solutions) has been performed by Durlofsky and Brady.[13] These authors, however, considered boundary conditions of the form,

$$H_{\lambda}(0)=H_{\lambda}''(0)=H_{\lambda}(1)=H_{\lambda}'(1)=0, \tag{6}$$

and thus restricted the analysis to symmetric perturbations.

A. Symmetric solutions

For symmetric solutions of type I with boundary conditions given by Eq. (6), Durlofsky and Brady found that $\lambda>1$ for all eigenvalues and $0<R<\infty$. Consequently, these solutions are stable under symmetric perturbations. However, this stability is marginal when $R\to\infty$ since the lowest eigenvalue tends to one. When general conditions (5) are chosen, antisymmetric perturbations are included in the analysis. In Fig. 3, eigenvalues corresponding to symmetric (dotted lines) and antisymmetric (full lines) eigenfunctions of Eq. (4) are plotted vs the Reynolds number. These results were obtained with a code based on spectral methods following the procedure used by Orszag[15] to analyze the temporal stability of

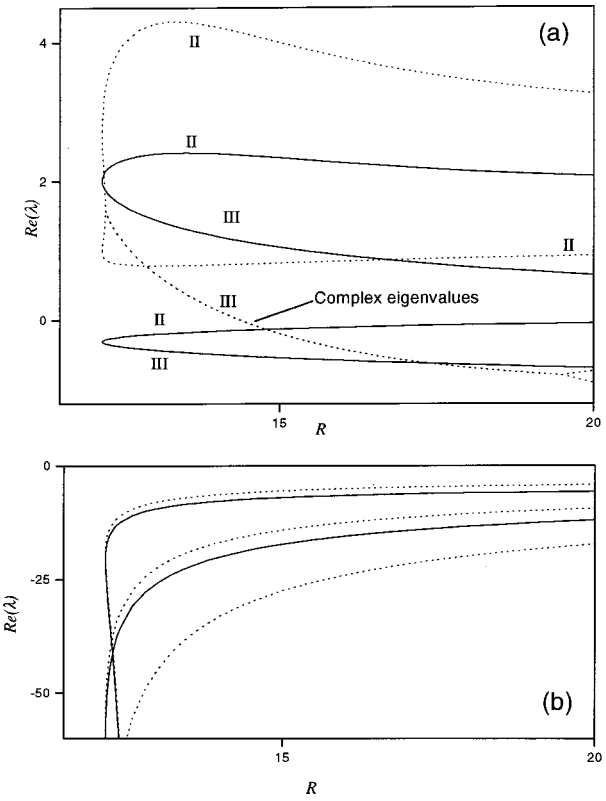

FIG. 4. (a) and (b) Real part of the eigenvalues of symmetric (type II and III) solutions of Eq. (3) corresponding to antisymmetric (full lines) and symmetric (dotted lines) eigenfunctions. Note the difference in the scale of the vertical axes. In (b), the branches in the upper right-hand corner are of type III. They merge with type II branches with flow reversal at the minimum value of $R=R_{\mathrm{II}}=12.165$.

Poiseuille flow. Half of the branches are those described in Ref. 13. The others are due to the antisymmetric perturbations. The lowest branch, and thus the one that determines the instability of the solution, corresponds to an antisymmetric eigenfunction. This branch crosses the line $\lambda=1$ at $R=R_{\mathrm{I}}$, which means that these solutions lose their temporal and spatial stability at the same value of the Reynolds number. This fact becomes apparent when the eigenvalue equation arising from the temporal stability analysis is considered (see Ref. 8). If temporal perturbations of the form $G(y)\exp(st)$ are proposed, the following characteristic value problem for the eigenfunctions G and the eigenvalues s is obtained,

$$G^{iv}+R(fG'''+f'''G-f''G'-f'G'')=sRG''. \tag{7}$$

For this kind of perturbations, there is an exchange of stability if $s=0$. A comparison between Eqs. (4) and (7) shows that, at a given R, a temporal mode with $s=0$ is also a spatial marginal mode ($\lambda=1$).

Consequently, the spatial stability of the symmetric solutions of type I is determined by the antisymmetric eigenvalues, and the range of Reynolds numbers for which these solutions are spatially stable coincides with the range of temporal stability.

The real part of the eigenvalues for symmetric (dotted lines) and antisymmetric (full lines) eigenfunctions of the other two symmetric solutions (types II and III) are plotted in

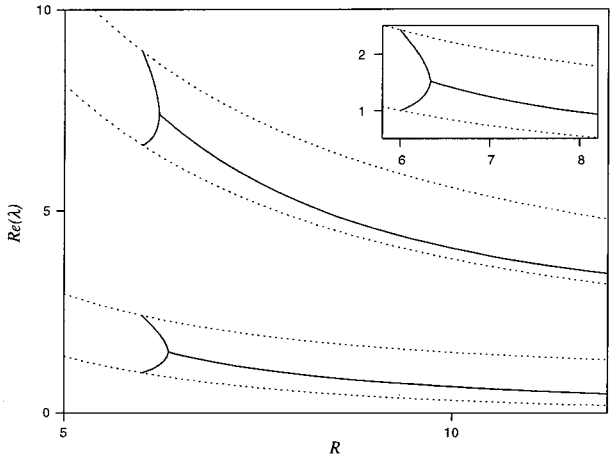

FIG. 5. Real part of the eigenvalues of symmetric (type I, dotted lines) and asymmetric (type I_a and I'_a, full lines) solutions of Eq. (3).

Figs. 4(a) and 4(b). Figure 4(a) shows the eigenvalues with minimum magnitude of $\mathrm{Re}(\lambda)$ corresponding to symmetric and antisymmetric eigenfunctions of solutions of types II and III. For type II solutions there is a branch of real eigenvalues with $0<\lambda\leqslant 1$, so that these solutions are unstable. Nevertheless, for large R, the instability of solutions of type II with respect to symmetric perturbations becomes marginal. In fact, all branches of type II eigenvalues coalesce with the corresponding ones of type I as $R\to\infty$. This behavior, which is linked to the presence of the cusp bifurcation at $R=\infty$ mentioned in Sec. II, can be observed comparing eigenvalues at $R=20$ in Figs. 3 and 4(a).

As in the case of type I solutions, the antisymmetric perturbations prove to be more dangerous for stability since the minimum magnitude eigenvalues are negative in this case. It is interesting to note in this figure that the structure of the spectrum is somewhat different from the one shown in Ref. 13 since complex eigenvalues, not considered in that paper, are included in Fig. 4 by plotting their real parts. This is exhibited in Fig. 4(a) as the merging of two real branches at the lower right hand corner, $R\sim 19.5$, and at $R\sim 12.2$.

Figure 4(b) presents branches with negative eigenvalues of larger magnitude. Note that the scale of the vertical axis is different from that of Fig. 4(a). The branches in the upper right hand corner of the figure correspond to type III solutions. They merge with type II branches with flow reversal at the minimum value of $R=R_{\mathrm{II}}=12.165$. These branches of type II solutions tend to $-\infty$ as the Reynolds number approaches the value $R'_{\mathrm{II}}=13.119$, which is the largest value of R for solutions of type II with flow reversal. The uppermost branch in this figure was already calculated in Ref. 13. The overall structure of this part of the spectrum for type II solutions is quite different from that of Fig. 4(a).

B. Asymmetric solutions

When the symmetric solution of type I loses its temporal stability, two asymmetric solutions which are mirror images of each other in the center line of the channel (types I_a and

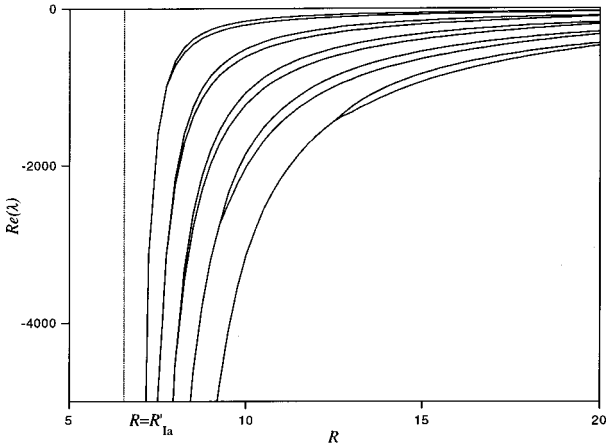

FIG. 6. Eigenvalues with large negative real part of asymmetric solutions of Eq. (3) with flow reversal. The eigenvalues diverge when the Reynolds number approaches the critical value $R'_{I_a}=6.557$.

I'_a) are generated in a pitchfork bifurcation. The temporal stability analysis for these solutions shows that they are stable for $R<R_{Ia}=12.963$.[8]

The asymmetric solutions are characterized by a displacement of the stagnation point towards one of the walls. The axial velocity increases near this wall and decreases near the other one. This asymmetry effect increases with the Reynolds number. When $R>R'_{Ia}=6.557$ there is a region close to one of the channel walls where the flow reverses.

Figure 5 shows the spectrum for both symmetric (type I, dotted lines) and asymmetric (type I_a and I'_a, full lines) solutions. The real part of the eigenvalues for the asymmetric solutions (solutions of type I_a and I'_a have the same spectrum) remains above unity if $R<R''_{Ia}=7.872$. However, the stability criteria for these flows become ambiguous when the flow reverses (i.e., when $R>R'_{Ia}$), as perturbations may be carried by the flow in both directions. In the presence of flow reversal there are new branches of eigenvalues (not plotted in Fig. 5) that are not present when $R<R'_{Ia}$. These branches, shown in Fig. 6, are characterized by eigenvalues with a large negative real part. Consequently, we may say that asymmetric solutions of type I_a and I'_a are stable if and only if there is no flow reversal in the channel, that is, if $R<R'_{Ia}$.

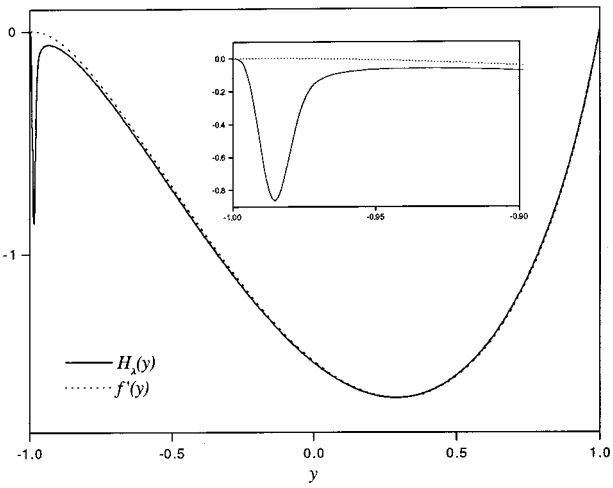

FIG. 7. Eigenfunction corresponding to an eigenvalue with large negative real part (full line). The Reynolds number $R=6.6$ is close to the critical value $R'_{I_a}=6.557$ where solutions with flow reversal first appear. The inset shows a detail in the region of flow reversal. Away from the boundary layer the solution is proportional to $f'(y)$ (dotted line).

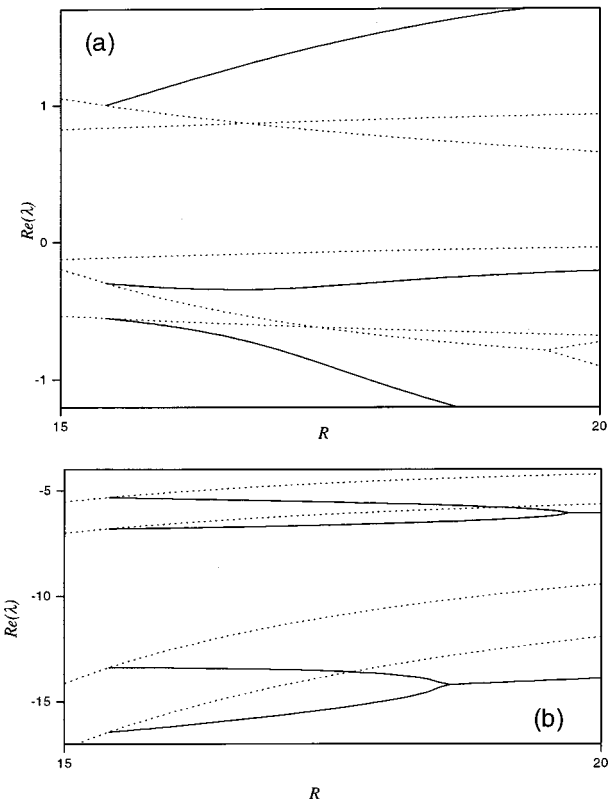

FIG. 8. (a) and (b) Real part of the eigenvalues of asymmetric solutions of Eq. (3) of types III_a and III'_a (full lines) and of symmetric one of types II and III (dotted lines). The scales and ranges of the vertical axis in (a) and (b) differ.

It is interesting to note that eigenvalues with a very large negative real part as those presented in Fig. 6 are found not only in solutions of type I_a, but also in symmetric solutions of type II near the point where the flow reverses ($R<R'_{II}$), as was shown in Fig. 4(b). These eigenvalues and their corresponding eigenfunctions were investigated analytically.[16] The analysis showed that the structure of the characteristic value problem depends strongly on the sign of $f''(y)$ at the points where $f'(y)$ vanishes. In Fig. 7 an eigenfunction of the solution of type I_a for $R=6.6$ is plotted. This value of the Reynolds number is close to the critical value $R'_{Ia}=6.557$, where flow reversal takes place. The modulus of the associated eigenvalue is as large as 10^6. The inset shows in more detail the structure of the boundary layer in the region of flow reversal close to the wall. Inside the channel the eigenfunction is proportional to $f'(y)$, with boundary layers at the walls, a property that can be derived from analytical considerations.[16]

The asymmetric solutions of types III_a and III'_a (the mirror image of III_a) were also investigated. They were found to be unstable under both symmetric and antisymmetric pertur-

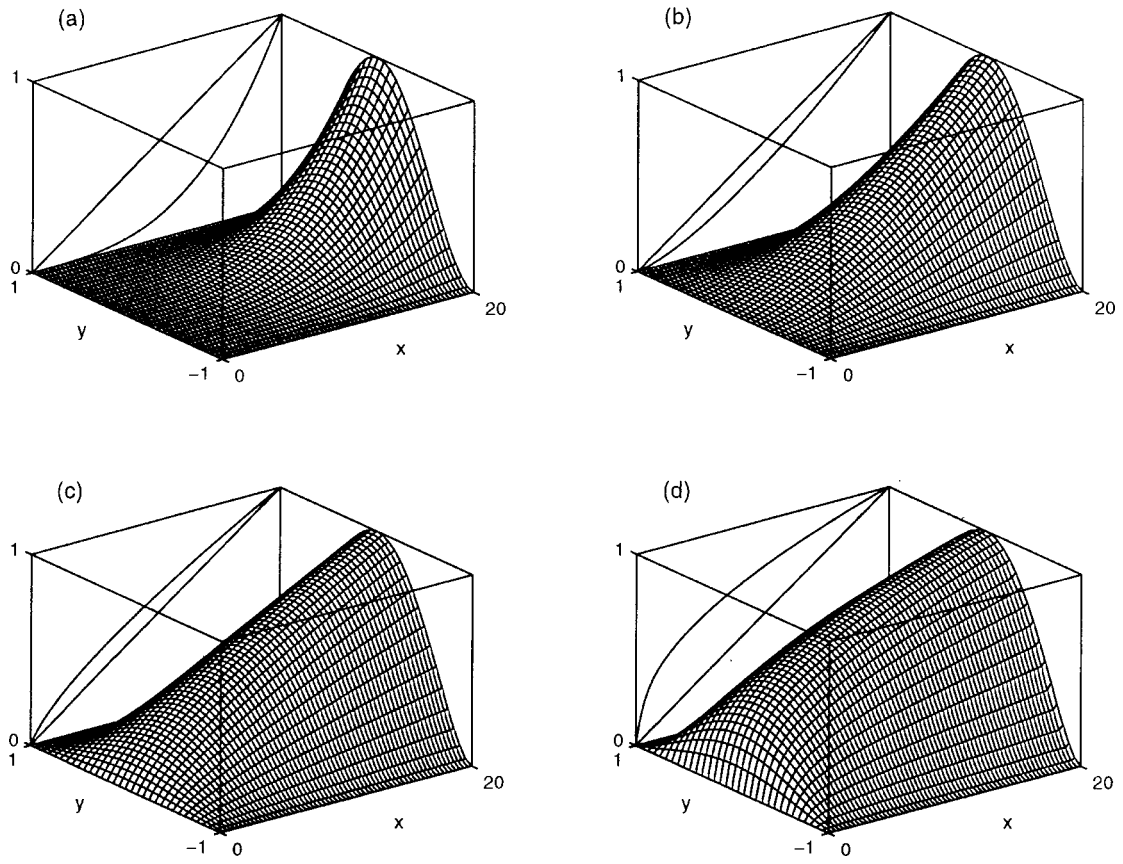

FIG. 9. Perturbations $\delta(x,y)=s(x,y)-xf(y)$ of similarity solutions defined by Eq. (3), for $L=20$; (a) $R=3$; (b) $R=5$; (c) $R=7$; (d) $R=9$. The stream function $s(x,y)$ was calculated using a bidimensional code. The conditions imposed at the mouth of the channel correspond to solutions of type I perturbed with their first eigenfunction. The two curves plotted on the $y=1$ plane are a straight line and the amplitude function $\Delta(x)=\max_y \delta(x,y)$.

bations. The results are shown in Figs. 8(a) and 8(b), where the real part of eigenvalues of type II and III solutions [already described in Figs. 4(a) and 4(b)] are plotted in dotted lines, and those of type III_a and III_a' in full lines. The minimum magnitude eigenvalues are presented in Fig. 8(a). As in Fig. 4, a different scale for the vertical axis is used in Fig. 8(b) to plot the eigenvalues with larger negative real part.

IV. FULLY BIDIMENSIONAL SOLUTIONS

In order to compare the spatially perturbed similarity solutions with fully bidimensional steady state ones, Eqs. (1) with no similarity assumptions were integrated numerically. A code in finite differences which solves the equations iteratively was developed. Multigrid and local relaxation techniques were employed to improve convergence. The problem has a new nondimensional parameter, L, the channel length given in terms of its half-width.

To complete the characterization of the problem, boundary conditions at both edges of the channel should be imposed. By assuming symmetry with respect to the $x=0$ axis, the domain is reduced to the $x>0$ half of the channel. The stream function and the vorticity are equal to zero at $x=0$. The conditions at the entrance, $x=L$, depend on the flow conditions outside the channel.

The vorticity-stream function representation was used and the system was discretized using centered finite differences over a uniform grid with 513 nodes in the x direction and 65 nodes in the y direction.

Boundary conditions of the form $f_c(y)=f(y)+\alpha H_\lambda(y)$, with $\alpha \ll 1$, were selected at the entrance of the channel. The functions $f(y)$ and $H_\lambda(y)$ are solutions of Eqs. (3) and (4), respectively.

In order to analyze the difference between a bidimensional solution and the similarity solution, the function $\delta(x,y)=s(x,y)-xf(y)$ is introduced, where $s(x,y)$ is the stream function as calculated by the bidimensional code. For the proposed boundary conditions, if the solution derived with the code resembles the similarity solution a behavior $\delta(x,y)\sim \alpha x^\lambda H_\lambda(y)$ is expected, except in the vicinity of the origin where Eq. (4) no longer holds.

Normalized functions $\delta(x,y)$ are presented together with their amplitudes $\Delta(x)=\max_y \delta(x,y)$, for $L=20$ and $R=3$, 5, 7, and 9 in Fig. 9. The conditions imposed at the mouth of the channel correspond to solutions of type I perturbed with their first eigenfunction. The two curves plotted on the $y=1$ plane are $\Delta(x)$ and a straight line that represents the linear behavior in x of the similarity solution. The surface plots show that for every value of x the perturbation conserves its profile. The amplitudes $\Delta(x)$ decay faster than the solution in the first two cases. This agrees with the fact that those cases correspond to stable solutions ($\lambda>1$). On the other hand, the last two graphs show a spatial attenuation that is smaller than the linear one of the similarity solution.

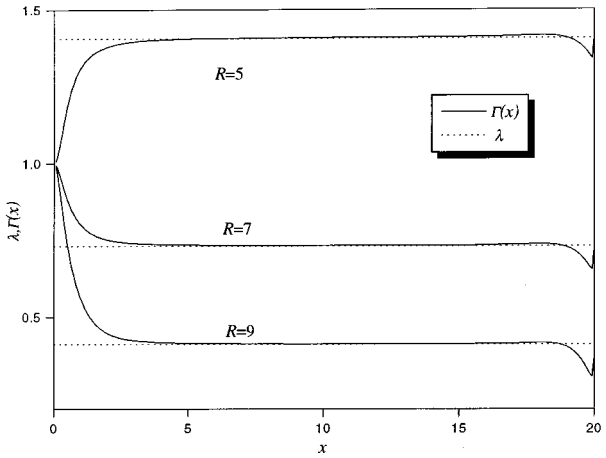

FIG. 10. Local attenuation rate $\Gamma(x)=d(\ln(\Delta)/d(\ln(x))$ of bidimensional perturbations compared to characteristic values λ provided by the linear analysis.

This is to be expected since for $R=7$ and 9 the similarity solutions are unstable.

In Fig. 10 the local attenuation rate of the solution, defined as $\Gamma(x)=d(\ln(\Delta)/d(\ln(x))$ (full lines), and the characteristic values λ (dotted lines) provided by the linear analysis are plotted. An excellent agreement is observed when the distance to the origin is more than three times the half-width of the channel. These results, commented in detail in Ref. 16, confirm the validity of the stability analysis.

V. CONCLUSIONS

Solutions of type I and I_a are the only branches of solutions of Berman's equation which are spatially stable for a certain range of Reynolds numbers. For solutions of type I the range of spatial stability is the same as the range of temporal stability. The instability threshold is determined by an antisymmetric perturbation. On the other hand, the range of spatial stability of the type I_a solutions is considerably shorter than the range of temporal stability. For this type of solutions the spatial stability is restricted to those solutions which have no flow reversal.

A singularity in the spectrum of solutions with flow reversal is present. Branches of eigenvalues with negative real part diverge as the Reynolds number approaches the critical value where solutions with flow reversal first appear.

Two-dimensional simulations of the flow in the channel were developed. These simulations were carried out with the aid of a finite difference code written in a vorticity-stream function formulation of the problem. The results given by this code support the validity of the linear stability analysis in the region not close to the center of the channel.

In conclusion, we have shown that the potential presence of antisymmetric perturbations considerably restricts the range of Reynolds numbers where similarity solutions are stable. There are stable similarity solutions for $R<6.557$ only. These solutions are symmetric if $R<6.001$ and asymmetric if $R>6.001$. However, it is important to keep in mind that in practical cases some unstable modes may not develop due to the finite length of the channel.

ACKNOWLEDGMENTS

This work was supported in part by Contract No. CTI*CT 91-0944 of the European Union, by the University of Buenos Aires (Grants Nos. EX088 and TX32), and by CONICET (Consejo Nacional de Investigaciones Cientificas y Técnicas).

[1] A. S. Berman, ''Laminar flow in channels with porous walls,'' J. Appl. Phys. **24**, 1232 (1953).
[2] R. D. Bundy and H. L. Weissberg, ''Experimental study of fully developed laminar flow in a porous pipe with wall injection,'' Phys. Fluids **13**, 2613 (1970).
[3] J. R. Sellars, ''Laminar flow in channels with porous walls at high suction Reynolds number,'' J. Appl. Phys. **26**, 489 (1955).
[4] S. W. Yuan, ''Further investigation of laminar flow in channels with porous walls,'' J. Appl. Phys. **27**, 267 (1956).
[5] I. Proudman, ''An example of steady laminar flow at large Reynolds number,'' J. Fluid Mech. **9**, 593 (1960).
[6] R. M. Terrill, ''Laminar flow in a uniformly porous channel,'' Aeronaut. Q. **15**, 299 (1964).
[7] W. A. Robinson, ''The existence of multiple solutions for the laminar flow in a uniformly porous channel with suction at both walls,'' J. Eng. Math. **10**, 23 (1976).
[8] M. B. Zaturska, P. G. Drazin, and W. H. H. Banks, ''On the flow of a viscous fluid driven along a channel by suction at porous walls,'' Fluid Dyn. Res. **4**, 151 (1988).
[9] S. M. Cox, ''Two-dimensional flow of a viscous fluid in a channel with porous walls,'' J. Fluid Mech. **227**, 1 (1991).
[10] A. D. MacGillivray and C. Lu, ''Asymptotic solution of a laminar flow in a porous channel with large suction: A nonlinear turning point problem,'' Meth. Appl. **1**, 229 (1994).
[11] S. M. Cox and A. C. King, ''On the asymptotic solution of a high-order nonlinear ordinary differential equation,'' Proc. R. Soc. London, Ser. A **453**, 711 (1997).
[12] C. Lu, ''On the asymptotic solution of laminar channel flow with large suction,'' SIAM (Soc. Ind. Appl. Math.) J. Math. Anal. **28**, 1113 (1997).
[13] L. Durlofsky and J. F. Brady, ''The spatial stability of a class of similarity solutions,'' Phys. Fluids **27**, 1068 (1984).
[14] C. Canuto, M. Y. Hussaini, A. Quarteroni, and T. A. Zang, *Spectral Methods in Fluid Dynamics* (Springer-Verlag, New York, 1988).
[15] S. A. Orszag, ''Accurate solution of the Orr–Sommerfeld stability equation,'' J. Fluid Mech. **50**, 689 (1971).
[16] S. Ferro, doctoral dissertation, University of Buenos Aires, 1998.